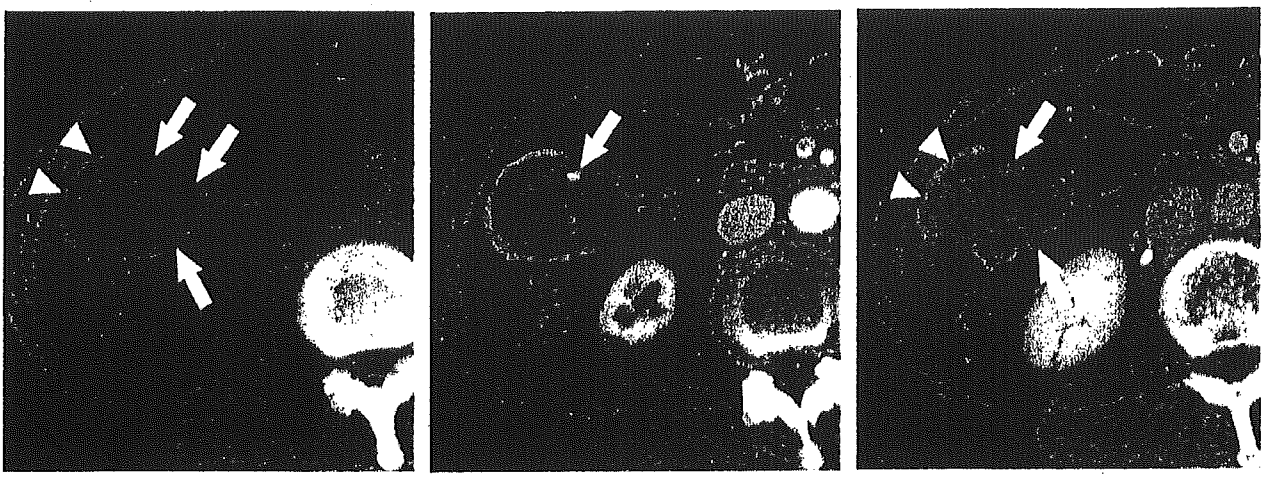


**Fig. 1.**
**A: Nonenhanced CT scan shows an exophytic mass of 5 cm in diameter in the right posterior inferior portion of the liver (*arrows*), and the liver parenchyma (*arrowheads*).**
**B: After intravenous administration of contrast material, arterial-phase CT shows a tiny enhancing dot (*arrow*) isoattenuating to aortic enhancement.**
**C: The main part of the tumor (*arrows*) shows heterogeneous enhancement hypoattenuating compared to that of liver parenchyma (*arrowheads*) on delayed images.**

ment centrally, with progressive enhancement on delayed images (Fig. 2).

Hepatic angiogram showed dilatation of the right posterior inferior branch of the hepatic artery and C-shaped opacification (Fig. 3).

Since we could not rule out malignant tumor based on these radiologic findings, partial resection of the liver was carried out. At surgery, a round tumor with capsule was seen, but no adhesion or peritoneal fluid was noted. The tumor was pedunculated and connected to the liver (subsegment 6) by a stalk of 3 cm in length. Macroscopically, the tumor measured 6.0×5.5×4.5 cm and was whitish, elastic, slightly firm, and well demarcated from the surrounding liver parenchyma. The cut surface of the tumor showed a whitish hyalinized area with dark red patches centrally and a tan-to-yellowish area peripherally (Fig. 4A). Histologically, there were multiple vessels of various sizes with marked hyaline-like degeneration in the central area, whereas small-sized vessels with rich fibrous stroma were predominant in the peripheral area (Figs. 4B, C). Somewhat large venous and arterial branches and large lymph vessels were seen in the border between the tumor and liver parenchyma. A pathological diagnosis of hepatic hemangioma was made.

The postoperative course was uneventful, and the patient was discharged 10 days after surgery.

## Discussion

Hemangioma is the most common benign tumor of the liver. The incidence of hemangioma in the general population varies in published reports from 0.4% to 20%.[1]

The typical radiologic features of cavernous hemangiomas have been well described, and it is usually easy to differentiate hemangioma from other liver tumors. However, the present case had atypical radiologic features, which caused some diagnostic confusion.

The typical US appearance is that of a homogeneous, hyperechoic mass with well-defined margins and some posterior echo enhancement.[2] In contrast to these features, in the present case, the internal echo pattern was partially hypoechoic and heterogeneous.

Strict criteria for the classic CT appearance of hepatic hemangioma include: relative hypoattenuation compared with normal liver on precontrast images, early peripheral enhancement, progressive spread of the opacified area towards the center of the lesion, and complete isoattenuating fill-in occurring not less than 3 minutes nor more than 60 minutes after contrast material administration.[3] Although the present tumor had a tiny enhancing dot in the arterial phase, early peripheral enhancement and progressive opacification towards the center of the lesion was not clear.

Hemangioma typically demonstrates marked high intensity on T2-weighted MR images and is usually spheroid or ovoid (87%).[3,4] However, the present tumor showed a moderately hyperintense and heterogeneous appearance on T2-weighted MR images.

In the present case, the hepatic angiogram showed dilatation of the right posterior inferior branch of the

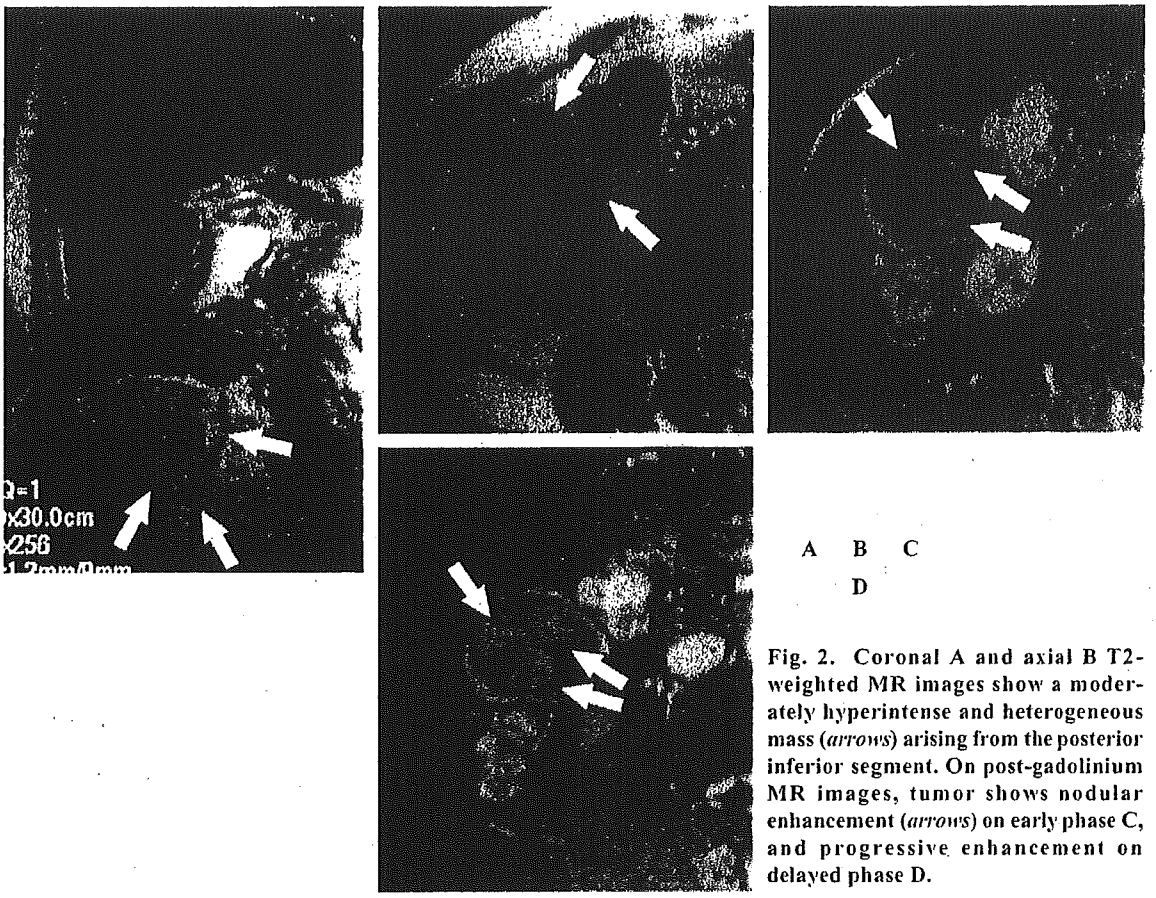


Fig. 2. Coronal A and axial B T2-weighted MR images show a moderately hyperintense and heterogeneous mass (*arrows*) arising from the posterior inferior segment. On post-gadolinium MR images, tumor shows nodular enhancement (*arrows*) on early phase C, and progressive enhancement on delayed phase D.

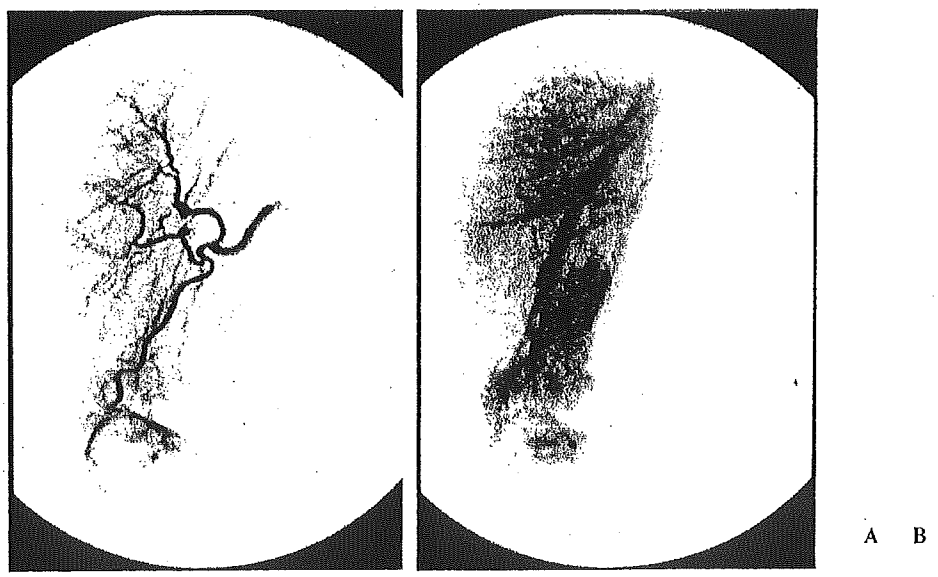


Fig. 3.
A: Selective hepatic angiogram shows dilatation of the right posterior inferior branch of the hepatic artery and C-shaped opacification.
B: Venous phase of hepatic angiogram shows mildly persistent peripheral enhancement.

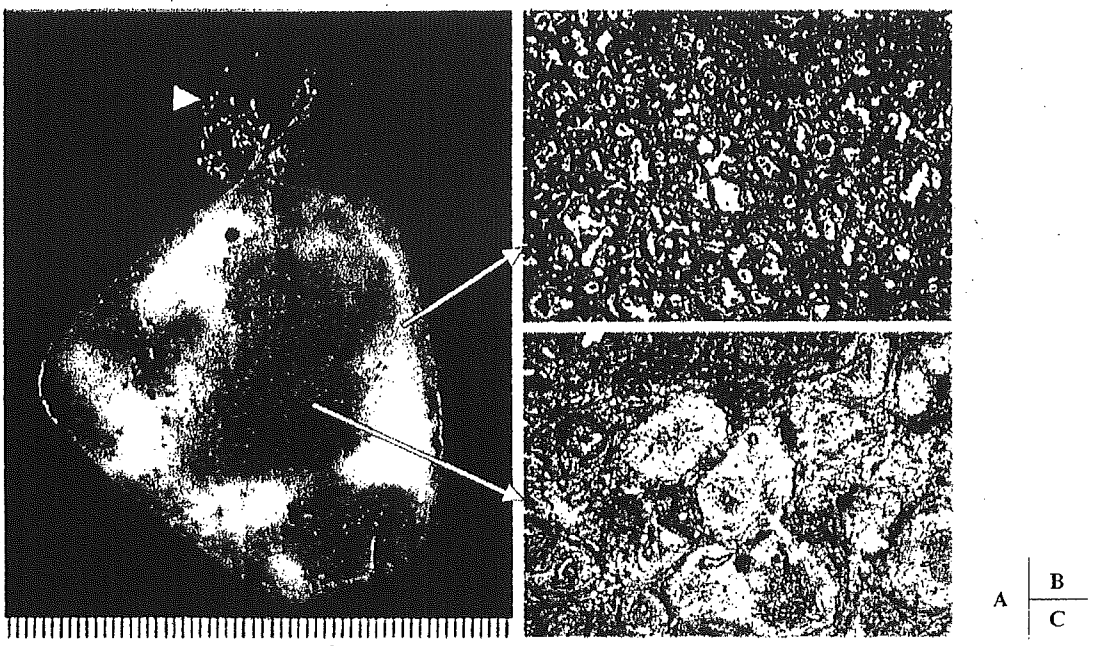


**Fig. 4.**
**A: The resected tumor is a 6.0×5.5×4.5 cm mass with a 3-cm-long stalk. The cut surface of the tumor shows the whitish hyalinized area with dark red patches centrally and the tan-to-yellowish area peripherally. The stalk is seen (*arrowhead*).**
**B: The peripheral area of the tumor shows small-sized vessels with rich fibrous stroma.**
**C: The central area shows multiple vessels of various sizes with marked hyaline-like degeneration (Hematoxylin-eosin stain, original magnification ×40).**

hepatic artery. Despite dilated feeding vessels, tumor vessels or vascular enhancement were not recognized. Dilated and tortuous feeding arteries are generally rare in hepatic hemangioma.[5]

The present tumor demonstrated radiologic findings inconsistent with those of typical hemangioma in all modalities. Nevertheless, this tumor showed a tiny enhancing dot in the arterial-phase CT scan that was considered to be consistent with the "bright dot" sign. Jang *et al.* advocated that this sign could be helpful in diagnosing small hemangiomas with nonspecific hypoattenuation at the arterial phase and portal venous phase of spiral CT.[6] In our case, there might have been a chance of a correct diagnosis preoperatively. However, the "bright dot" sign is characteristic of small hemangiomas (<2 cm in diameter), and it is uncertain whether this sign is reliable for large hemangiomas like our case (>4 cm in diameter). Further experience is needed.

The surgical procedure for benign hepatic tumors has been controversial. Terkivatan *et al.* reported that they advised surgery for any benign hepatic tumor that caused severe complaints and when there was an uncertain diagnosis.[7] In the present case, since the patient was asymptomatic, a radiologic follow-up or percutaneous needle biopsy might have been a reasonable option. However, we selected resection for the uncertain hepatic tumor because of its relatively large diameter, risk of rupture of the exophytic lesion, and the inability to exclude malignancy.

Histopathologically, multiple vessels of various sizes, remarkable hyalinization, and fibrosis of the stroma were present without a cavernous pattern in our case. The pathological diagnosis of hemangioma was based on the presence of variably sized, endothelial-lined vascular channels.

We considered various reasons for these atypical radiologic features. First, remarkable hyalinization and fibrosis without a cavernous pattern of the tumor can be causative of minimal enhancement. Some investigators reported that the reasons for nonenhancement of hemangioma were slow flow in the central sinusoids, central fibrosis, central thrombosis, and hemorrhage.[5,8] Yamashita *et al.* advocated that enhancement patterns and hemodynamic characteristics of hemangiomas could vary depending on the internal architecture of the lesion.[9] Second, the current tumor presented an exophytic appearance. According to Brancatelli *et al.*, 12% of hemangiomas demonstrate exophytic growth.[1] Moreover, pedunculated hemangiomas are very rare.[10] Third, the relatively large size of the present tumor could have

been the reason for atypical radiologic findings. Hepatic hemangiomas are typically less than 3 cm in diameter. When larger than 4 cm, Nelson *et al.* classified them as "giant hemangioma".[3] Generally, on dynamic contrast-enhanced CT scans, delayed imaging of large hemangioma shows further centripetal enhancement, however, complete filling with contrast material has never been observed.[11] Large hemangioma has a spectrum of histopathologic changes, including hemorrhage, thrombosis, extensive hyalinization, liquefaction, and fibrosis.[5,8,11] These features cause a heterogeneous appearance on MR images. There occasionally exists confusion in distinction between giant hemangioma and malignant tumors including necrotic metastatic tumor and hepatocellular carcinoma.[11] In fact, although the present tumor had no cystic degeneration, it was difficult to exclude those malignant hepatic tumors beforehand. Furthermore, primary hepatic angiosarcoma should be added to the differential diagnosis when dynamic CT and MR imaging show heterogeneous enhancement on early-phase images and progressive enhancement on delayed images.[12]

Some authors have suggested that hyalinized hemangiomas represent an end stage of hemangioma involution.[13] This case might therefore be regarded as an incomplete stage to hyalinization.

In summary, our report documents an unusual radiologic manifestation of hepatic hemangioma. Hemangioma should be considered in the differential diagnosis when a tumor shows a large heterogeneous mass with a tiny enhancing dot, even if the tumor is pedunculated.

## References


1) Brancatelli G, Federle MP, Blachar A, Grazioli L. Hemangioma in the cirrhotic liver: diagnosis and natural history. *Radiology*, 219: 69–74, 2001.
2) Moody AR, Wilson SR. Atypical hepatic hemangioma: a suggestive sonographic morphology. *Radiology*, 188: 413–417, 1993.
3) Nelson RC, Chezmar JL. Diagnostic approach to hepatic hemangiomas. *Radiology*, 176: 11–13, 1990.
4) Tung GA, Vaccaro JP, Cronan JJ, Rogg JM. Cavernous hemangioma of the liver: pathologic correlation with high-field MR imaging. *AJR Am J Roentgenol*, 162: 1113–1117, 1994.
5) Takayasu K, Moriyama N, Shima Y, *et al.* Atypical radiographic findings in hepatic cavernous hemagioma: correlation with histologic features. *AJR Am J Roentgenol*, 146: 1149–1153, 1986
6) Jang HJ, Choi BI, Kim TK, *et al.* Atypical small hemangiomas of the liver: "bright dot" sign at two-phase spiral CT. *Radiology*, 208: 543–548, 1998.
7) Terkivatan T, de Wilt JH, de Man RA, *et al.* Indications and long-term outcome of treatment for benign hepatic tumors: a critical appraisal. *Arch Surg*, 136: 1033–1038, 2001.
8) Johnson CM, Sheedy PF 2nd, Stanson AW, Stephens DH, Hattery RR, Adson MA. Computed tomography and angiography of cavernous hemangiomas of the liver. *Radiology*, 138: 115–121, 1981.
9) Yamashita Y, Ogata I, Urata J, Takahashi M. Cavernous hemangioma of the liver: pathologic correlation with dynamic CT fingings. *Radiology*, 203: 121–125, 1997.
10) Bader TR, Braga L, Semelka RC. Exophytic benign tumors of the liver: appearance on MRI. *Magn Reson Imaging*, 19: 623–628, 2001.
11) Choi BI, Han MC, Park JH, Kim SH, Han MH, Kim CW. Giant cavernous hemangioma of the liver: CT and MR imaging in 10 cases. *AJR Am J Roentgenol*, 152: 1221–1226, 1989.
12) Koyama T, Fletcher JG, Johnson CD, Kuo MS, Notohara K, Burgart LJ. Primary hepatic angiosarcoma: findings at CT and MR imaging. *Radiology*, 222: 667–673, 2002.
13) Vilgrain V, Boulos L, Vullierme MP, Denys A, Terris B, Menu Y. Imaging of atypical hemangiomas of the liver with pathologic correlation. *Radiographics*, 20: 379–397, 2000.

# Prediction of Lung Adenocarcinoma Without Vessel Invasion*

## A CT Scan Volumetric Analysis

*Ukihide Tateishi, MD, PhD; Hajime Uno, PhD; Kan Yonemori, MD; Mistuo Satake, MD; Masahiro Takeuchi, ScD, MPH; and Yasuaki Arai, MD, PhD*

***Study objectives:*** **Patients with lung adenocarcinoma without vessel invasion have a favorable prognosis after resection and are among the candidates for limited surgery. The purpose of the present study was to predict lung adenocarcinoma without vessel invasion based on a volumetric analysis of the lesion with a CT scan prior to the operation.**

***Methods:*** **CT scan images were obtained in 288 consecutive patients with adenocarcinoma of the lung before surgical resection. Total tumor volume, the volume of the nonsolid component, and the proportion occupied by the nonsolid component were calculated by the perimeter method. The performance of the derived logistic regression model and the volumetric results were evaluated by receiver operating characteristic analysis. The model derived for the prediction of tumors without vessel invasion was assessed by means of the leave-one-out cross-validation technique.**

***Results:*** **The pathologic diagnosis was adenocarcinoma with vessel invasion in 160 cases, and without vessel invasion in 128 cases. The median total tumor volume, the median volume of the nonsolid component, and median proportion occupied by the nonsolid component were 1,123.7 $mm^3$, 253.4 $mm^3$, and 58.0%, respectively. With the derivation of the predictive rule, stepwise regression yielded the following five features: the proportion occupied by the nonsolid component; spiculation; pleural indentation; gender; and tumor size. The Az value, a measure of diagnostic power represented as the area under the curve, was 0.957 for prediction of lung adenocarcinoma without vessel invasion. The cross-validation accuracy achieved by applying the rule was 90.3%.**

***Conclusions:*** **The proportion occupied by the nonsolid component based on a CT scan volumetric analysis was a reliable predictor of tumors without vessel invasion in patients with adenocarcinoma of the lung.**

*(CHEST 2005; 128:3276–3283)*

**Key words:** CT scan; lung; lung cancer

**Abbreviations:** CI = confidence interval; OR = odds ratio; ROC = receiver operating characteristic; SPN = solitary pulmonary nodule

Patients with lung adenocarcinoma without vessel invasion clearly have the best outcome after resection, and they are among the candidates for limited surgery.[1,2] Some studies[3,4] have highlighted the potential diagnostic role of thin-section CT scanning in identifying nonsolid components of adenocarcinoma of the lung. The nonsolid component is larger in patients with noninvasive tumors and has been shown to discriminate between patients with noninvasive tumors and patients with advanced tumors with a high degree of power.[5] In addition, the proportion of the tumor occupied by the nonsolid component correlates well with the absence of vascular or lymphatic invasion and with better outcome.[6–10] Thus, identification of the size of the nonsolid component on CT scan images of lung adenocarcinoma is a potential surrogate measurement for tumor aggressiveness.

The reliability of almost all data on the proportion

*From the Division of Diagnostic Radiology (Drs. Tateishi, Yonemori, Satake, and Arai), National Cancer Center Hospital, Tokyo, Japan; the Department of Biostatistics (Dr. Uno), Harvard School of Public Health, Boston, MA; and the Division of Biostatistics (Takeuchi), Kitasato University Graduate School, Tokyo, Japan.

Dr. Uno received support for this research by Banyu Life Science Foundation International.

Manuscript received January 12, 2005; revision accepted May 4, 2005.



*Correspondence to: Ukihide Tateishi, MD, PhD, Division of Diagnostic Radiology, National Cancer Center Hospital, Tsukiji, Chuo-Ku, 104-0045, Tokyo, Japan; e-mail: utateish@ncc.go.jp*

occupied by the nonsolid component is limited, because the investigators assumed that the lesions were spherical and used the maximum cross-sectional diameter on CT scan images to calculate it,[5,6] and the only large series to date used the maximum cross-sectional area of the tumor to predict invasion.[11] To our knowledge, few studies have used CT scanning to calculate the volume of the nonsolid component within tumors and to correlate the proportion occupied by the nonsolid component with pathologic characteristics of tumor invasion. Moreover, most studies to date have proposed diagnostic criteria for lesions without testing their diagnostic validity.[6–11]

We therefore conducted both a derivation and validation cohort study of patients with adenocarcinoma of the lung in order to predict tumors without vessel invasion. Our results will assist physicians in estimating more accurately the probability of a tumor being unassociated with vessel invasion and to decide whether further investigation is necessary to rule the presence of a noninvasive tumor in or out.

## Materials and Methods

A retrospective review of the pathologic records for the period between October 2001 and January 2004 identified 288 who had been patients treated for adenocarcinoma of the lung the maximum dimension of which was < 2 cm. A consecutive subset of 288 patients contributed to the derivation analysis and the cross-validation analysis based on the leave-one-out method. The study population consisted of 113 men and 175 women, and their mean age was 64.7 years (age range, 41 to 86 years). All patients had undergone surgical resection consisting of wedge resection or lobectomy. Complete dissection (n = 96; 33%) and sampling of mediastinal or hilar lymph nodes (n = 192; 67%) were performed. The nodes included high and low ipsilateral, paratracheal, subcarinal, and inferior pulmonary ligament lymph nodes, and any other suspicious lymph nodes identified at surgery. Surgical specimens were fixed in formalin and embedded in paraffin. Four-micrometer sections were stained with hematoxylin and eosin and elastica-van Gieson stain. Tumors without vessel invasion were diagnosed when no lymphatic or blood vessel invasion was identified within the lesion microscopically. Based on the current international TNM classification for staging lung cancer,[12] 274 tumors (95%) were classified as stage Ia, and the other 14 tumors (5%) were classified as stage IIa. The clinical records of all patients were available for review. No patients were lost to follow-up, which began on the date of the initial operation. The median duration of follow-up was 22 months, and ranged from 1 to 40 months. This study was approved by our institutional review board after confirmation of informed consent by the patients to a review of their records and images.

CT scanning was performed with a multidetector scanner (Aquilion V-detector; Toshiba Medical Systems; Tokyo, Japan) by using axial 2.0-mm × 4 or 1.0-mm × 16 modes (*ie*, 4 or 16 images per gantry rotation), 120 kVp, 200 to 250 mA, and a 0.5-s scanning time. Thin-section CT scan images were obtained using 2.0-mm sections that were reconstructed at 2.0-mm intervals by means of a high-spatial frequency algorithm and were retrospectively retargeted to each lung with a 20-cm field of view. All images were displayed at window settings for lung (center, −600 Hounsfield units; width, 2,000 Hounsfield units). Image viewing and manipulation were controlled with a workstation (ZIOSOFT M900, Quadra, version 3.10f; ZIOSoft Inc; Tokyo, Japan) that allows the reader to draw lines through regions of interest and the perimeters around them.

The CT scan images were assessed in random order by two independent observers without reference to the clinical findings. The observers examined the images for the following: maximum tumor diameter; nodular edge (irregular or not); presence of a nonsolid component; presence of an air-bronchogram; presence of cavitation, lobulation, pleural indentation, bubble-like lucencies, spiculation, vascular convergence, bronchiectasis, or bronchiolectasis; and the lobe in which the lesion was located (*eg*, upper, middle, or lower). *Nonsolid component* was defined as an area of ground-glass attenuation or hazy increased parenchymal attenuation without obscuring of the underlying vascular markings. We distinguished between *nonsolid tumors* and *part-solid tumors*, with the former being defined as tumors containing only a nonsolid component, and the latter as tumors that contained a partially solid component. Bubble-like lucencies were diagnosed when there were multiple cystic air spaces measuring ≤ 5 mm in diameter within the lesion surrounded by a wall of variable thickness.[13] After an initial independent evaluation, the two observers reviewed all cases in which their interpretations disagreed and reached a final decision by consensus.

The volume of each tumor was calculated by the perimeter method.[14–16] The cross-sectional areas of the entire tumor and of the solid component were calculated by a workstation that manipulates a voxel matrix of 512 × 512 pixels. Two board-certified radiologists who were experienced with image-viewing and image-manipulation software drew a line around the perimeter of each tumor twice. The total tumor volume and the volume of the solid component were calculated by summing the cross-sectional areas and multiplying by the section increment. The volume of the nonsolid component was calculated by subtracting the volume of the solid component from the total volume. The averages of the two volume values calculated by each of the two observers were used in the analyses.

### *Statistical Analysis*

Interobserver variation in relation to CT scan findings was quantified as the weighted κ coefficient of agreement. The predictive performance of volumetric data was evaluated by receiver operating characteristic (ROC) analysis, and the areas under curve were represented by the Az values, which are a measure of diagnostic power represented by the area under the curve.[17,18] A stepwise procedure was used in the logistic regression analysis to select the independent variables that should have been included in the model to predict tumors without vessel invasion. A variable was entered into the model if the probability of its score statistic was < 0.05. The odds ratio (OR) and 95% confidence interval (CI) for the multivariate predictors were estimated. The Hosmer-Lemeshow test was also performed to evaluate goodness-of-fit.[19] Calibration curves comparing the observed proportion of tumors without vessel invasion with the probability of tumors without vessel invasion ordered by the increasing probability of tumors without vessel invasion were constructed. The performance of the learned model was verified by using the leave-one-out cross-validation method, in which all cases but one were used to train the prediction rule, which was then applied to the single excluded case.[20–22] This procedure was repeated for each case, until each case had been left out only once. Cross-validation accuracy was calculated by comparing the predicted response and the observed response.[23] The following variables were considered for their prognostic value: age; gender;

**Table 1—*Patient Demographics**

| Characteristics | No Vessel Invasion (n = 128) | Vessel Invasion (n = 160) |
|---|---|---|
| Gender | | |
| Male | 39 (30) | 74 (46) |
| Female | 89 (70) | 86 (54) |
| Age,† yr | | |
| Mean | 64 | 65.4 |
| SD | 9.1 | 8.8 |
| Range | 41–84 | 41–86 |
| Location of tumor | | |
| Upper lobe | 78 (61) | 91 (57) |
| Middle lobe | 14 (11) | 5 (3) |
| Lower lobe | 36 (28) | 64 (40) |
| Tumor size,† mm | | |
| Mean | 12.4 | 15.8 |
| SD | 4.5 | 3.5 |
| Range | 5.0–20.0 | 7.0–20.0 |
| Tumor with nonsolid component | 124 (97) | 78 (49) |
| Nonsolid tumor | 81 (63) | 1 (1) |
| Part-solid tumor | 43 (34) | 77 (48) |
| Solid tumor | 4 (3) | 82 (51) |

*Values are given as No. (%).

†The differences between two groups were assessed by a two-sample *t* test. The two tumor subgroups differed significantly in terms of gender (p 0.01 [$\chi^2$ test]). Tumors without vessel invasion were significantly more frequent (p 0.01 [$\chi^2$ test]) in the upper lobe than those with vessel invasion. Tumor size was significantly smaller in tumors without vessel invasion (p 0.01 [*t* test]) than that in tumors with vessel invasion. Tumors with a nonsolid component were significantly more frequent (p 0.0001 [$\chi^2$ test]) among tumors without vessel invasion.

presence or absence of vessel invasion; tumor size; total tumor volume; the volume of the nonsolid component; the proportion occupied by the nonsolid component; and CT scan findings. Univariate analysis was performed by comparing Kaplan-Meier disease-free or recurrence-free survival curves and carrying out log-rank tests. All analyses were conducted using a statistical software package (SAS, version 8.2; SAS Institute, Cary, NC; and R software, version 1.9.0; R project, Center for Computational Intelligence; Vienna, Austria).

## Results

The clinical characteristics and outcomes of all patients with adenocarcinoma of the lung are summarized in Table 1. The pathologic diagnosis was lung adenocarcinoma with vessel invasion in 160 of the 288 patients (55.6%), and without vessel invasion in the other 128 patients (44.4%). Female patients had a predilection for tumors without vessel invasion according to the results of the univariate analysis. The median age at presentation was 66 years (age range, 41 to 86 years). Age was not statistically associated with tumor type. Most tumors (n = 169; 58.7%) were in the upper lobe. The median tumor size was 15.0 mm (range, 5.0 to 20.0 mm). Tumors with vessel invasion were significantly larger than tumors without vessel invasion. Among the tumors without vessel invasion, nonsolid tumors (n = 81; 28.1%) were more common than part-solid or solid tumors (n = 47; 16.3%); whereas, among the tumors with vessel invasion, solid or part-solid tumors (n = 159; 55.2%) were more common than nonsolid tumors (n = 1; 0.3%). Tumors with a nonsolid component were more common among the tumors without vessel invasion than among the tumors with vessel invasion.

There was good interobserver agreement in the analysis of the CT scan findings (weighted $\kappa$ coefficient, 0.63 to 0.79). The following CT scan findings were more frequently identified in tumors with vessel invasion than in tumors without vessel invasion according to the univariate analysis: cavitation; air bronchogram;

**Table 2—*Summary Statistics of Volumetric Measurements**

| Variables | No Vessel Invasion | Vessel Invasion |
|---|---|---|
| Tumor volume, $mm^3$ | | |
| Mean | 1,155.7 | 1,773.6 |
| SD | 1,411.1 | 1,321.3 |
| Q1-Median-Q3 | 247.6–713.8–1,544.6 | 867.1–1,492.5–2,367.4 |
| Range | 43.6–6,828.0 | 120.8–6,912.2 |
| Volume of nonsolid component, $mm^3$ | | |
| Mean | 1,027.5 | 496.9 |
| SD | 1,372.7 | 829.6 |
| Q1-Median-Q3 | 157.5–567.7–1,413.3 | 0.0–0.0–658.5 |
| Range | 0.0–6,593.4 | 0.0–4583.6 |
| Proportion of nonsolid component, % | | |
| Mean | 88.1 | 24.3 |
| SD | 26.4 | 33.2 |
| Q1-Median-Q3 | 93.4–100.0–100.0 | 0.0–0.0–41.4 |
| Range | 0.0–100.0 | 0.0–100.0 |

*The differences between two groups were assessed by the Wilcoxon two-sample *t* test. The tumor subgroups differed significantly in terms of the volume of those three kinds of measurements (p 0.0001). Q1 = 25th percentile; Q3 = 75th percentile.

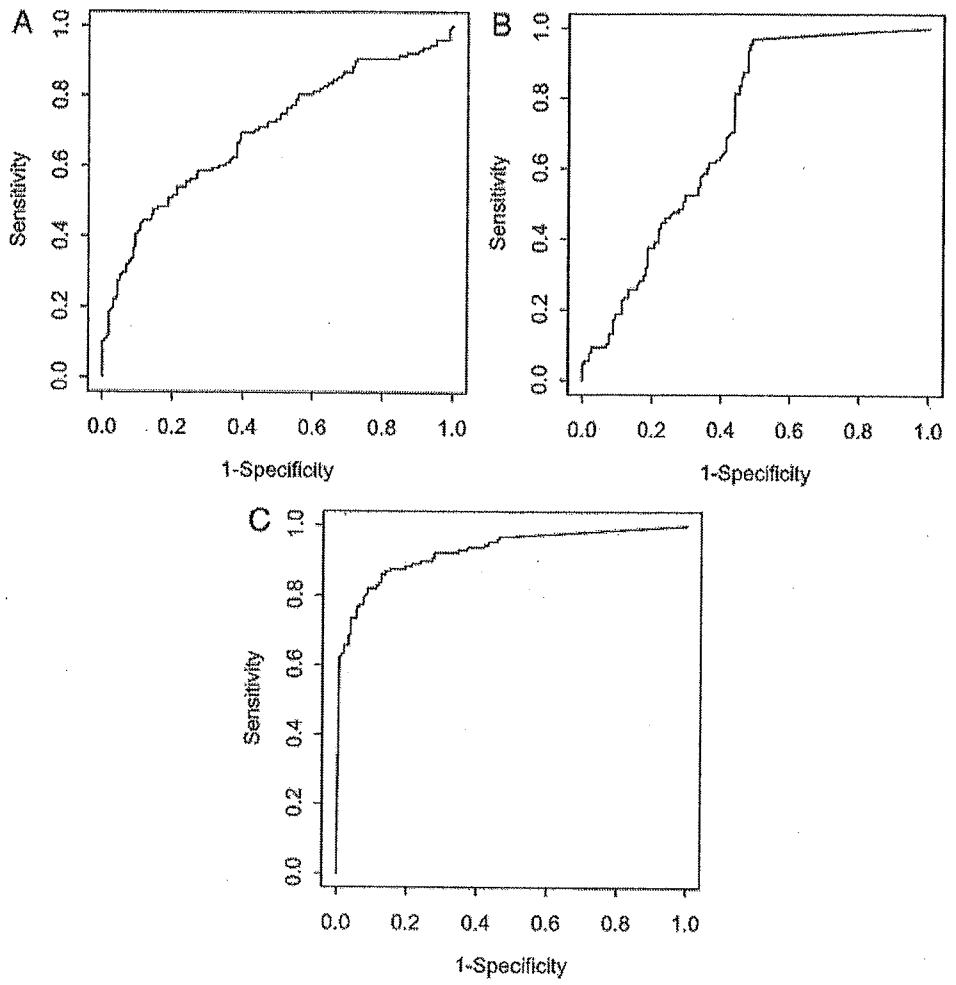


FIGURE 1. *Top*, *A*: ROC curve for total tumor volume determined by the perimeter method. The mean (± SE) Az value was 0.699 ± 0.030. *Middle*, *B*: the ROC curve for the volume of the nonsolid component determined by the perimeter method. The mean Az (± SE) value was 0.714 ± 0.030. *Bottom*, *C*: ROC curve for the proportion occupied by the nonsolid component determined by the perimeter method. The mean Az (± SE) value was 0.928 ± 0.015.

irregular margin; speculation; lobulation; and bronchiectasis or bronchiolectasis. Irregular margins were common in tumors without vessel invasion but were more frequent in tumors with vessel invasion. Vascular convergence was a less common finding and was noted only in patients with tumors that were associated with vessel invasion. Bubble-like lucencies were observed in one tumor with vessel invasion and in one tumor without vessel invasion.

*Volumetric Analysis*

The results of the volumetric analysis are summarized in Table 2. The median total tumor volume, the median volume of the nonsolid component, and the median proportion occupied by the nonsolid component were 1,123.7 $mm^3$ (range, 43.6 to 6,912.2 $mm^3$), 253.4 $mm^3$ (range, 0 to 6,593.4 $mm^3$), and 58.0% (range, 0 to 100%), respectively. Significant differences were found between the mean values for total volume and the proportion values in two groups. The ROC analyses to predict tumors without vessel invasion revealed that Az values of total tumor volume, the volume of the nonsolid component, and the proportion occupied by the nonsolid component were 0.699 (95% CI, 0.638 to 0.760), 0.714 (95% CI, 0.653 to 0.775), and 0.928 (95% CI, 0.895 to 0.961), respectively (Fig 1). The potential predictors of tumors without vessel invasion at the threshold of each median value were as follows: total tumor volume; the volume of the nonsolid component; and the proportion occupied by the nonsolid component (Table 3). Univariate analysis showed that our pre-

**Table 3—*Potential Predictors of Tumors Without Vessel Invasion**

| Criteria | Proportion of Tumors Without Vessel Invasion, % | OR | 95% CI | p Value† |
|---|---|---|---|---|
| Gender | | 1.9636 | 1.2053–3.1992 | 0.0064 |
| Female | 50.9 | | | |
| Male | 34.5 | | | |
| Age | | 1.1124 | 0.6983–1.7723 | 0.6543 |
| ≤ 66 yr | 45.7 | | | |
| > 66 yr | 43.1 | | | |
| Tumor size | | 4.0588 | 2.4416–6.7472 | < 0.0001 |
| ≤ 15 mm | 58.5 | | | |
| > 15 mm | 25.8 | | | |
| Air bronchogram | | 0.1143 | 0.0585–0.2235 | < 0.0001 |
| Positive | 13.6 | | | |
| Negative | 58.0 | | | |
| Irregular margin | | 0.1605 | 0.0636–0.4049 | < 0.0001 |
| Positive | 40.1 | | | |
| Negative | 80.6 | | | |
| Spiculation | | 0.0349 | 0.0159–0.0767 | < 0.0001 |
| Positive | 7.1 | | | |
| Negative | 68.6 | | | |
| Lobulation | | 0.1496 | 0.0185–1.2122 | 0.0412 |
| Positive | 11.1 | | | |
| Negative | 45.5 | | | |
| Pleural indentation | | 0.1148 | 0.0673–0.1961 | < 0.0001 |
| Positive | 21.2 | | | |
| Negative | 70.1 | | | |
| Bubble-like lucencies | | 1.2540 | 0.1742–9.0269 | 0.8221 |
| Positive | 50.0 | | | |
| Negative | 44.4 | | | |
| Vascular convergence | | NA | NA | < 0.0001 |
| Positive | 0.0 | | | |
| Negative | 50.0 | | | |
| Bronchiectasis or bronchiolectasis | | 0.2150 | 0.0468–0.9882 | 0.0312 |
| Positive | 15.4 | | | |
| Negative | 45 | | | |
| Tumor volume | | 2.9934 | 1.8465–4.8528 | < 0.0001 |
| ≤ 1,123.7 $mm^3$ | 57.6 | | | |
| > 1,123.7 $mm^3$ | 31.3 | | | |
| Volume of nonsolid component | | 2.6535 | 1.6431–4.2853 | < 0.0001 |
| > 253.4 $mm^3$ | 56.3 | | | |
| ≤ 253.4 $mm^3$ | 32.6 | | | |
| Proportion of nonsolid component | | 42.778 | 21.5856–84.7761 | < 0.0001 |
| > 80% | 84.6 | | | |
| ≤ 80% | 11.4 | | | |

*The median value was considered to be a cutoff in age, tumor size, tumor volume, the volume of the nonsolid component, and the proportion of the nonsolid component. NA = not applicable.
†$\chi^2$ test.

dictor of interest, the proportion occupied by the nonsolid component, was highly predictive of tumors without vessel invasion at an OR of 42.8 (95% CI, 21.6 to 84.8) with 80.0% as the threshold value.

*Derivation of the Prediction Rule*

From the 13 variables that reached the level of statistical significance in the univariate analyses comparing tumors with and without vessel invasion, we excluded location of the tumor because the absolute difference fell within the precision range of the test.

The logistic regression analysis identified the following five significant predictors of tumors without vessel invasion: proportion occupied by the nonsolid component; spiculation; pleural indentation; gender; and tumor size (Table 4). The Az value of the ROC analysis for prediction of a tumor without vessel invasion in the derivation phase was 0.957 (Fig 2). We adopted the threshold that yielded an appropriate tradeoff between sensitivity and specificity (*ie*, probability of a tumor without vessel invasion, 0.5). At that point in the ROC curve, the sensitivity, specificity, accuracy, positive predictive value, and

Table 4—*Significant Predictors of Tumors Without Vessel Invasion*

| Variables | Coefficient | OR* | 95% CI | p Value |
|---|---|---|---|---|
| Intercept | −1.6729 | | | |
| Proportion of nonsolid component > 80% vs ≤ 80% | 3.5744 | 35.673 | 14.392–88.421 | < 0.0001 |
| Positive vs negative spiculation | −2.3889 | 0.092 | 0.032–0.261 | < 0.0001 |
| Positive vs negative pleural indentation | −1.3982 | 0.247 | 0.101–0.602 | 0.0021 |
| Female vs male gender | 1.0056 | 2.734 | 1.141–6.551 | 0.0241 |
| Tumor size ≤ 15 mm vs > 15.0 mm | 1.1271 | 3.087 | 1.249–7.627 | 0.0146 |

*OR was presented to predict tumors without vessel invasion.

negative predictive value of the rule were 88.3%, 91.9%, 90.3%, 89.7%, and 90.7%, respectively. The results of the goodness-of-fit test ($\chi^2$, 3.6563; degrees of freedom, 8; $p = 0.89$) indicated that the observed proportion of patients with tumors without vessel invasion was similar to the predicted proportion in the derivation group. The calibration curves for the derivation data demonstrated good calibration of the prediction rule.

*Cross-Validation Accuracy*

When the rule derived from the 288 patients was applied to the leave-one-out cross-validation cohort, the validation accuracy based on the leave-one-out method was 90.3%, which was quite similar to the model accuracy, suggesting that the rule that was derived to predict tumors without vessel invasion is stable.

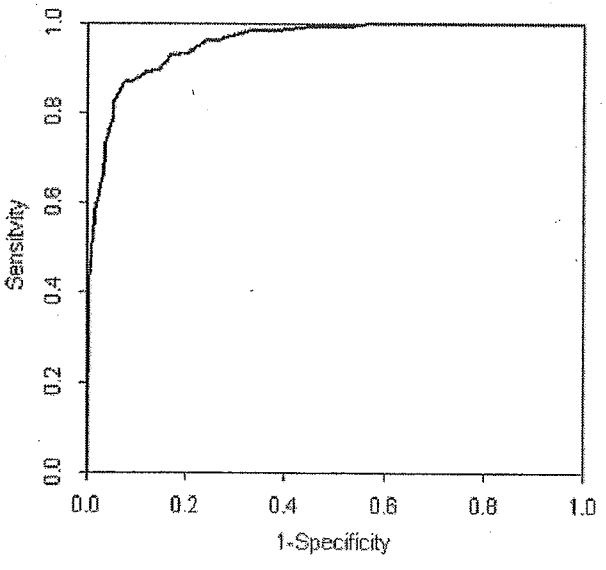


FIGURE 2. ROC curve for the derived model to predict tumor without vessel invasion. The probability of the occurrence of a tumor without vessel invasion based on the derived model can be considered diagnostic, and the tradeoff between sensitivity and specificity at various thresholds of the probability of a tumor without vessel invasion is given by the ROC curve.

*Prognostic Analysis*

At the last follow-up, 1 of the 288 patients (0.3%) had died, 12 patients (4.2%) were alive with recurrent disease, and the 5-year overall survival rate was 98.7%. Univariate analysis revealed that none of the variables had a significant impact on overall survival. The 5-year recurrence-free survival rate was 83.5%. The patients with tumors without vessel involvement had a 5-year recurrence-free rate of 88.0%, which was significantly better than the rate of 74.6% among the patients with vessel invasion ($p < 0.05$). Cavitation and vascular convergence were significantly associated with recurrence-free survival according to the univariate analysis ($p < 0.01$).

## Discussion

The proportion occupied by the nonsolid component is characteristically higher in patients with lung adenocarcinoma without vessel invasion, and several studies[4,5] have demonstrated that it distinguishes tumors without vessel invasion from tumors with vessel invasion. Nevertheless, controversy remains regarding its reproducibility in optimally distinguishing tumors without vessel invasion from tumors with vessel invasion. In this study, we investigated the diagnostic capacity of the proportion occupied by the nonsolid component to predict tumors without vessel invasion in a well-characterized study population.

We performed ROC analysis to assess the ability of the proportion occupied by the nonsolid component to discriminate between tumors with and without vessel invasion. We have documented that the diagnostic probability of the proportion occupied by the nonsolid component for tumors without vessel invasion is accurate. The Az value observed for the proportion occupied by the nonsolid component was 0.957. In our study population, its discriminatory capacity yielded positive and negative predictive values for tumors without vessel invasion of 89.7% and 90.7%, respectively. These observations suggest that the identification of the proportion occupied by the nonsolid component on CT images may be useful

for predicting tumors without vessel invasion in patients with adenocarcinoma of the lung.

At both baseline screenings and repeat CT screenings for lung cancer, tumors containing a nonsolid component have been found to be a significant sign of malignancy.[24] Henschke and colleagues[25] found that 19% of the 233 cases with positive results at baseline screening had a tumor with the nonsolid component and that the tumors were predominantly bronchioloalveolar carcinoma and adenocarcinoma with bronchioloalveolar carcinoma features. These predominant histologic types of malignancy corresponded to noninvasive and invasive tumors of lung adenocarcinoma. The quantification of the extent or growth rate of the solid and nonsolid components of tumors is necessary during CT scan screening for lung cancer.

Swensen and colleagues[18] created a multivariate logistic regression model to predict a malignant solitary pulmonary nodule (SPN) in a derivation and validation analysis. Of 629 radiologically intermediate nodules in their study, 23% were malignant SPNs. The investigators identified the following three independent findings that predicted malignant SPNs: upper lobe distribution; tumor size; and spiculation. Among these findings, spiculation was associated with the prediction model in our results. Pleural indentation and male predilection were also significant predictors of tumors with vessel invasion in our study.

Some studies[26–28] using the segmentation algorithm of software have yielded calculations of tumor volume in three dimensions. The excellent interobserver variability suggests that tumor volume estimations by different observers can be reliably compared when three-dimensional volumetric software is used. However, this technique does not enable the segmentation of tumors that contain a nonsolid component.[27,28] Since most tumors in our study contained a nonsolid component and were not appropriate for three-dimensional volumetric analysis, tumor volume was calculated by the perimeter method, which had potential sources of error that affected the results of volumetric analyses.[29]

The proportion occupied by the nonsolid component was dichotomized using the median value for a threshold level in the univariate and multivariate analyses performed. In both the univariate and multivariate analyses, the proportion occupied by the nonsolid component yielded the highest point estimates and CIs for the ORs of tumors without vessel invasion. However, it should be noted that there was enough of a difference between the values for patients in whom the nonsolid component occupied a high proportion of the tumor and those for patients in whom the nonsolid component occupied a small proportion of the tumor that similar results could have been obtained with different threshold values.

There are other potential limitations of this study. The size of the sample may also have led to false-positive results because of the number of covariates included in the initial analysis. However, the strength of the association with our primary outcome of interest, as well as the historical precedence of other significant predictors in our multivariate analysis, lends credence to our conclusions. In summary, the results of our study confirm that the proportion occupied by the nonsolid component of a tumor on CT scans is a reliable predictor of tumors without vessel invasion with much greater confidence than was possible in the past.

## References


1 Travis WD, Colby TV, Corrin B, et al. Histological typing of lung and pleural tumors. Berlin, Germany: Springer, 1999

2 Noguchi M, Morikawa A, Kawasaki M, et al. Small adenocarcinoma of the lung: histologic characteristics and prognosis. Cancer 1995; 75:2844–2852

3 Jang HJ, Lee KS, Kwon OJ, et al. Bronchioloalveolar carcinoma: focal area of ground-glass attenuation at thin-section CT as an early sign. Radiology 1996; 199:485–488

4 Kuriyama K, Seto M, Kasugai T, et al. Ground-glass opacity on thin-section CT: value in differentiating subtypes of adenocarcinoma of the lung. AJR Am J Roentgenol 1999; 173:465–469

5 Ohde Y, Nagai K, Yoshida J, et al. The proportion of consolidation to ground-glass opacity on high resolution CT is a good predictor for distinguishing the population of non-invasive peripheral adenocarcinoma. Lung Cancer 2003; 42: 303–310

6 Aoki T, Tomoda Y, Watanabe H, et al. Peripheral lung adenocarcinoma: correlation of thin-section CT findings with histologic prognostic factors and survival. Radiology 2001; 220:803–809

7 Suzuki K, Yokose T, Yoshida J, et al. Prognostic significance of the size of central fibrosis in peripheral adenocarcinoma of the lung. Ann Thorac Surg 2000; 69:893–897

8 Kodama K, Higashiyama M, Yokouchi H, et al. Prognostic value of ground-glass opacity found in small lung adenocarcinoma on high-resolution CT scanning. Lung Cancer 2002; 33:17–25

9 Matsunaga H, Yokoi K, Anraku M, et al. Proportion of ground-glass opacity on high-resolution computed tomography in clinical T1N0M0 adenocarcinoma of the lung: a predictor of lymph node metastasis. J Thorac Cardiovasc Surg 2002; 124:278–284

10 Kim EA, Johkoh T, Lee KS, et al. Quantification of ground-glass opacity on high-resolution CT of small peripheral adenocarcinoma of the lung: pathologic and prognostic implications. AJR Am J Roentgenol 2001; 177:1417–1422

11 Takashima S, Maruyama Y, Hasegawa M, et al. Prognostic significance of high-resolution CT findings in small peripheral adenocarcinoma of the lung: a retrospective study on 64 patients. Lung Cancer 2002; 36:289–295

12 Lababede O, Meziane MA, Rice TW. TNM staging of lung cancer: a quick reference chart. Chest 1999; 115:233–235

13 Adler B, Padley S, Miller RR, et al. High-resolution CT of bronchioloalveolar carcinoma. AJR Am J Roentgenol 1992; 159:275–277

14 Winter-Muram HT, Jennings SG, Tarver RD, et al. Volumetric growth rate of stage I lung cancer prior to treatment: serial CT scanning. Radiology 2002; 223:798–805
15 Winter-Muram HT, Jennings SG, Meyer CA, et al. Effect of varying CT section width on volumetric measurement of lung tumors and application of compensatory equations. Radiology 2003; 229:184–194
16 Jennings SG, Winter-Muram HT, Tarver RD, et al. Lung tumor growth: assessment with CT-comparison of diameter and cross-sectional area with volume measurements. Radiology 2004; 231:866–871
17 Hanley JA, McNeil BJ. The meaning and use of the area under a receiver operating characteristic (ROC) curve. Radiology 1982; 143:29–36
18 Swensen SJ, Silverstein MD, Ilstrup DM, et al. The probability of malignancy in solitary pulmonary nodules: application to small radiologically intermediate nodules. Arch Intern Med 1997; 157:849–855
19 Lemeshow S, Hosmer DW. A review of goodness-of-fit statistics for use in the development of logistic regression models. Am J Epidemiol 1982; 115:92–106
20 Wasson JH, Sox HC, Neff RK, et al. Clinical prediction rules: applications and methodological standards. N Engl J Med 1985; 313:793–799
21 Scott JA. Pulmonary perfusion patterns and pulmonary arterial pressure. Radiology 2002; 224:513–518
22 Arana E, Delicado P, Marti-Bormati L. Validation procedures in radiologic diagnostic models: neural network and logistic regression. Invest Radiol 1999; 34:636–642
23 Stone M. Cross-validatory choice and assessment of statistical predictions. J R Stat Soc B 1974; 36:111–147
24 Henschke CI, McCauley DI, Yankelevitz DF, et al. Early lung cancer action project: overall design and findings from baseline screening. Lancet 1999; 354:99–105
25 Henschke CI, Yankelevitz DF, Mircheva R, et al. CT screening for lung cancer: frequency and significance of part-solid and nonsolid nodules. AJR Am J Roentgenol 2002; 1178: 1053–1057
26 Yankelevitz DF, Reeves AP, Kostis WJ, et al. Small pulmonary nodules: volumetrically determined growth rates based on CT evaluation. Radiology 2000; 217:251–256
27 Revel MP, Lefort C, Bissery A, et al. Pulmonary nodules: preliminary experience with three-dimensional evaluation. Radiology 2004; 231:459–466
28 Revel MP, Bissery A, Bienvenu M, et al. Are two-dimensional CT measurements of small noncalcified pulmonary nodules reliable? Radiology 2004; 231:453–458
29 Staron RB, Ford E. Computed tomographic volumetric calcification reproducibility. Invest Radiol 1986; 21:272–274

Skelet Radiol
DOI 10.1007/s00256-005-0021-0

SCIENTIFIC ARTICLE

**Ukihide Tateishi**
**Tadashi Hasegawa**
**Takayuki Nojima**
**Tsutomu Takegami**
**Yasuaki Arai**

# MRI features of extraskeletal myxoid chondrosarcoma

Received: 23 February 2005
Revised: 13 May 2005
Accepted: 27 July 2005


All authors of this research paper have directly participated in the planning, execution, or analysis of the study
The contents of this manuscript have not been copyrighted or previously published
There are no directly related manuscripts or abstracts, published or unpublished, by any authors of this paper

U. Tateishi (✉) · Y. Arai
Division of Diagnostic Radiology,
National Cancer Center Hospital,
5-1-1, Tsukiji, Chuo-Ku,
104-0045 Tokyo, Japan
e-mail: utateish@ncc.go.jp
Tel.: +81-3-35422511
Fax: +81-3-35423815

T. Hasegawa
Department of Clinical Pathology,
Sapporo Medical University
School of Medicine,
Sapporo, Japan

T. Nojima
Department of Pathology,
Kanazawa Medical University,
Ishikawa, Japan

T. Takegami
Division of Molecular Oncology
and Virology,
Medical Research Institute,
Kanazawa Medical University,
Ishikawa, Japan

**Abstract** *Objective:* To describe the MRI features of extraskeletal myxoid chondrosarcoma in comparison with clinicopathologic findings. *Design and patients:* The study comprised 12 male subjects and seven female subjects with a mean age of 53 years (range 16–76 years). MRI findings, evaluated by two radiologists with agreement by consensus, were compared for histopathologic features. *Results:* The tumor size ranged from 2.0 cm to 20.0 cm (mean 8.9 cm). Fusion gene transcripts could be detected in 13 (68%) of the 19 cases: EWS-CHN in nine cases, TAF2N-CHN in three, and TFG-TCH in one. There were six fusion-negative cases. Signal characteristics on T1-weighted and T2-weighted MR images were non-specific with regard to each cytogenetic variant. Peripheral enhancement was seen more frequently in tumors with the EWS-CHN variant than in those with other cytogenetic variants. The characteristic pattern of enhancement corresponded to the presence of fibrous septa and peripheral areas of high cellularity within lobules, by correlation with pathologic findings. All cases with TAF2N-CHN or TFG-TCH variants showed invasion of extracompartmental structure, bone, or vessels. *Conclusion:* Extraskeletal myxoid chondrosarcoma is an uncommon soft-tissue malignancy that may be recognized by MRI features of multilobular soft-tissue mass often invading extracompartmental, bony, and vascular structures.

**Keywords** Extraskeletal myxoid chondrosarcoma · MRI · Cytogenetic variant

## Introduction

Extraskeletal myxoid chondrosarcoma (EMC) is a rare malignant soft-tissue tumor characterized by abundant myxoid matrix and malignant chondroblastic cells [1, 2]. EMC mostly arises in the deep soft tissue of the proximal extremities and limb girdles and comprises multiple gelatinous nodules divided by fibrous septa. Although the most common manifestation is an enlarging soft-tissue mass, some lesions are accompanied by pain and tenderness or may restrict the range of motion. Long-term follow-up studies have shown that EMC is a slowly growing tumor with a risk of local recurrence or distant metastasis. EMC is a tumor with long survival but is known to have a potential for local recurrence, metastasis, and a disease-associated death [1–4].

EMC was described as a distinct entity, precisely, by Enzinger and Shiraki [5]. Subsequent clinicopathologic

and molecular studies have yielded findings consistent with the distinct tumor characteristics and have revealed that EMC is composed of at least four cytogenetic variants: EWS-CHN, TAF2N-CHN, TCF12-CHN, TFG-TCH [6–11]. These variants were derived from independent chromosomal translocations and the resultant fusion genes. The identification of the highly specific balanced chromosomal rearrangement in EMC assists a specific diagnosis at molecular level.

The typical radiographic manifestation of EMC is that of a large, well-demarcated mass, partially contained by pseudocapsule, with associated intratumoral cysts and hemorrhage. A few reports on case series of EMC had been published at the time this article was written [12–14]. In addition, the relationship between cytogenetic variants and imaging findings were not fully understood.

The purpose of our study was to describe the imaging features of EMC in comparison with clinicopathologic findings.

## Materials and methods

Nineteen cases of EMC were retrieved from the pathology files of our institute. Patients were identified from a pathologic registration system database through a query for patients with diagnosed EMC who had undergone surgical resection. A reference pathologist reviewed all cases to confirm the histologic diagnosis based on current standards. Clinical information was extracted from the patient files regarding patient age, gender, symptoms, treatment, local recurrences, metastases, metastatic sites, associated conditions, and final disease status. Our institutional review board does not require its approval or patients' informed consent for this type of review.

Radiologic studies of each lesion were reviewed by two radiologists, with consensus, and included CT, with ($n$=4) and without ($n$=15) contrast material enhancement, and MRI with high-field (1.5-T) units in all patients. T1-weighted and T2-weighted images were obtained in the transverse plane and in at least one longitudinal plane with either a surface coil ($n$=15) or a body coil ($n$=4). T1-weighted fast spin-echo images were obtained by using a 24–30 cm field of view, 4–8 mm section thickness, 400–620 ms/8.9–15 ms repetition time/echo time, 256×192–224 matrix, two signals acquired. T2-weighted fast spin-echo acquisitions were performed by using a 24–35 cm field of view, 4–8 mm section thickness, 3,000–6,220 ms/84–120 ms repetition time/echo time, 256×192–224 matrix, two signals acquired. After the intravenous administration of 0.1 mmol of gadopentate dimeglumine (Magnevist, Schering, Berlin, Germany) per kilogram of body weight, transverse T1-weighted images with fat suppression were obtained in the transverse plane and in at least one longitudinal plane.

Images were evaluated for lesion location and size, depth (superficial or deep), shape of margin (well-defined or ill-defined), and the presence or absence of extracompartmental extension. Mineralized matrix was assessed on CT images. MR images were evaluated for predominant signal intensity characteristics (low, intermediate, or high), signal homogeneity or heterogeneity, as well as enhancement characteristics. On T1-weighted images low signal intensity was defined as signal intensity less than that of muscle; intermediate signal intensity, similar to that of muscle; and high signal intensity, similar to that of fat. On T2-weighted images, low signal intensity was defined as signal intensity similar to that of muscle; intermediate signal intensity, greater than that of muscle but less than that of fat; and high signal intensity, equal to or greater than that of fat. Tumor enhancement was visually graded as greater than, less than, or equal to, that of surrounding muscle and vessels. The pattern and homogeneity of enhancement were also recorded: peripheral, diffuse, and mixed patterns. Peripheral enhancement was assigned when the curvilinear enhancing septal areas were present within tumor. Cortical destruction and vascular encasement were also evaluated.

For reverse-transcribed polymerase chain reaction (RT-PCR) analysis, frozen tissues were available from 18 patients. The RNA was reverse transcribed, and the samples were then subjected to protein chain reaction (PCR) amplification using primers: CCCACTAGTTACCCAC CCCA (EWS exon 7 forward); TCTGGCAGACTTCTTT TAAGCA (EWS exon 11 forward); GCGATGCCACAGT GTCCTATG (EWS exon 12 forward); GAGCAGTCAA ATTATGATCAGCAGC (TAF2N forward); GCAACA ACGCATGGCCGCTAT (TCF12 forward); AGCTTGG AACCACCTGGAGAACC (TFG forward); GCTGTAT GTCTGCGCCGCATAACT (CHN-1 reverse); TCTCAG CCTCCGCTGGAGAGA (CHN-2 reverse). Specimens were fixed with formalin and sectioned in the same plane as that of the CT and MR images. The specimens were stained with hematoxylin–eosin, and immunohistochemical staining was also performed. In one patient whose frozen tissue was not available, fluorescence in situ hybridization (FISH) was performed to detect EWS gene aberrations in formalin-fixed paraffin-embedded tissue. Tumor specimens were immunostained with the antibody Ki-67 (Dako; diluted 1:100 and autoclaved), and the Ki-67 (MIB-1) labeling index (LI) was estimated by determining the percentage of Ki-67-positive cell nuclei per 1,000 tumor cells in the region of the tumor with the greatest density of ki-67 staining viewed under a light microscope. Both MIB-1 grade (MIB-1 grading system) and mitosis grade (the modified French system) are three-grade systems obtained by summing the scores of tumor differentiation, tumor necrosis, and the MIB-1 score or mitotic score, each of which was given a score of 0, 1, 2,or 3. Tumor differentiation score, according to histologic type, was modified slightly from the French system. The mitotic figures were counted on routine hematoxylin and eosin

**Table 1** Cytogenetic variants of EMC (*T1WI* T1-weighted image, *T2WI* T2-weighted image, *NOS* not otherwise specified

| Variant | Translocation | Number | T1WI | T2WI | Gadolinium enhancement | Extracompartmental extension | Bone invasion | Vascular invasion |
|---|---|---|---|---|---|---|---|---|
| EWS-CHN | t(9;22) (q22;q12) | 9 | Intermediate: 6 | Intermediate: 1 | Peripheral: 5 | 2 | 3 | 1 |
| TAF2N-CHN | t(9;17) (q22;q11) | 3 | High: 3<br>Intermediate: 2 | High: 8<br>High: 3 | Mixed: 4<br>Diffuse: 2 | 2 | 0 | 1 |
| TFG-TCH | t(3;9) (q11;q22) | 1 | High: 1<br>High: 1 | Intermediate: 1 | Mixed: 1<br>Mixed: 1 | 0 | 1 | 0 |
| NOS | – | 6 | Intermediate: 6 | Intermediate: 2<br>High: 4 | Mixed: 3<br>Diffuse: 2<br>Peripheral: 1 | 1 | 1 | 2 |

stained sections. The areas selected for cell counting were from the most mitotically active parts of the tumors, usually located at the periphery. The mitotic score was assessed by counting the number of mitotic figures in ten consecutive high-power fields. The MIB-1 score was estimated by counting the percentage of MIB-1-positive cell nuclei per 1,000 tumor cells in the region of the tumor with the greatest density of staining, which, in most instances, corresponded to the areas with the highest mitotic activity. In this study the histological grade of a tumor was determined by a three-grade system in which tumor differentiation, tumor necrosis, and MIB-1 LI, were each given a score of 0, 1, 2, or 3 and then added together. Lesions with MIB-1 LIs of 0–9%, 10–29%, or greater than 30% were assigned MIB-1 scores of 1,2 or 3, respectively. The three separate scores were added together to produce a combined grade: lesions with a total score of 2 or 3 were classified as grade 1, those that scored 4 or 5 were grade 2, and those that scored 6,7 or 8 were grade 3. According to this MIB-1 system, tumors were assigned grades 1–3. The cut surface, internal characteristics, and microscopic findings of the lesions were compared with those seen on CT and MR images. Correlation between the imaging and histologic findings was made by consensus between the radiologist and pathologist.

Follow-up information was available in all cases. Deaths confirmed to be caused by disease were treated as an end point, whereas deaths from other causes were treated as censored observations. The disease-free date was considered to be the date when the medical record documented no

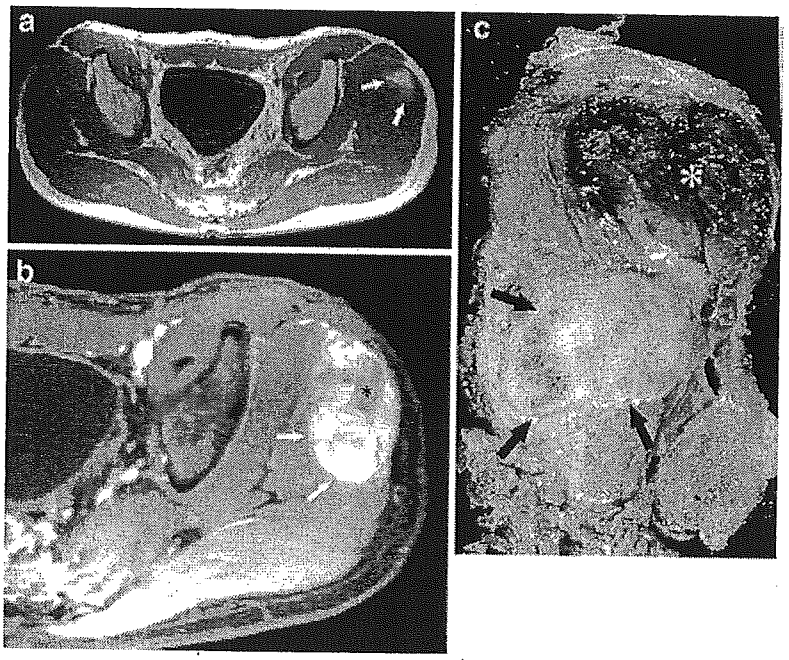


**Fig. 1** A 46-year-old man with the TAF2N-CHN variant of EMC arising from the left gluteal region. **a** Transverse, T1-weighted (500 ms/15 ms), MR image shows a focus of high signal intensity within the tumor (*arrows*), resulting from hemorrhage. **b** Transverse, fat-saturated, T1-weighted (600 ms/12 ms), MR image after contrast enhancement demonstrates moderate enhancement of the tumor. The enhancement of hemorrhagic areas (*asterisk*) was depicted more heterogeneously than those of solid portions (*arrows*). **C** Sectioned gross specimen reveals hemorrhagic areas (*asterisk*) and solid portions (*arrows*) admixed with extensive myxoid stroma corresponding to the MRI appearance

evidence of disease. Recurrence was assigned when the patient developed recurrent tumor related to surgical margins. Metastasis was assigned when the patient developed distant a metastasis, including bone and lung metastases, during the course of the disease and did not contain the case with recurrence.

## Results

There were 12 male (63%) and seven female (37%) patients aged from 16 years to 76 years, with an average age of 53 years. The arising sites of soft-tissues were calf ($n$=5), foot ($n$=4), buttock ($n$=3), thigh ($n$=3), groin ($n$=1), shoulder ($n$=1), arm ($n$=1), and hand ($n$=1). Presenting symptoms were stated in all patients. The most common symptom was a mass that had enlarged ($n$=15). Four patients had evidence of pain or tenderness. There were three cytogenetic variants in 13 cases (68%): EWS-CHN in nine cases, TAF2N-CHN in three, and TFG-TCH in one, and not otherwise specified in six cases (Table 1). There were 11 grade 1 tumors and eight grade 2 tumors as assigned by the MIB-1 grading system.

The mean diameter of tumors was 8.9 cm (range 2.0–20.0 cm). The location of the tumor was superficial in four patients (27%), while the remaining 11 (73%) were distributed deeply. Mineralized matrix that was centrally located within the tumor was seen in one case on non-enhanced CT images. Multi-nodular soft-tissue masses with well-defined ($n$=5, 26%) or ill-defined ($n$=14, 74%) margins were seen on CT and MR images. One patient (5%) demonstrated a metastatic lesion at initial presentation.

MR images showed predominantly intermediate ($n$=14, 74%) and high ($n$=5, 26%) signal intensity relative to muscle on T1-weighted MR images, with one lesion also demonstrating areas of focal high signal intensity, reflecting the hemorrhagic region (Fig. 1). On T2-weighted MR images, signal intensity was heterogeneous in all patients. Fifteen lesions (79%) had high signal intensity, equal to or greater than that of fat. The remaining four lesions (21%) had intermediate signal intensity, greater than that of muscle but less than that of fat. Signal characteristics on T1-weighted and T2-weighted MR images were non-specific with regard to each cytogenetic variant.

All lesions demonstrated mild-to-moderate and heterogeneous enhancement of the tumor after intravenous administration of a gadolinium-based contrast agent. Solid components of the tumors showed peripheral enhancement ($n$=6, 32%, Fig. 2), diffuse enhancement ($n$=4, 21%, Fig. 3), and a mixed pattern of enhancement ($n$=9, 47%). Peripheral enhancement was seen more frequently in tumors with the EWS-CHN variant than in those with other cytogenetic variants ($P$<0.05).

Ulceration of the tumor surface was identified in one case. Vascular encasement was seen in four cases, and one of those cases was accompanied by intravenous tumor extension. Tumors showed extracompartmental extension in five patients. Cortical destruction with soft-tissue mass was seen in five patients. Of these, a tumor arising from the back showed intraforaminal extension to the spinal canal, with marked bone destruction. All cases with TAF2N-CHN

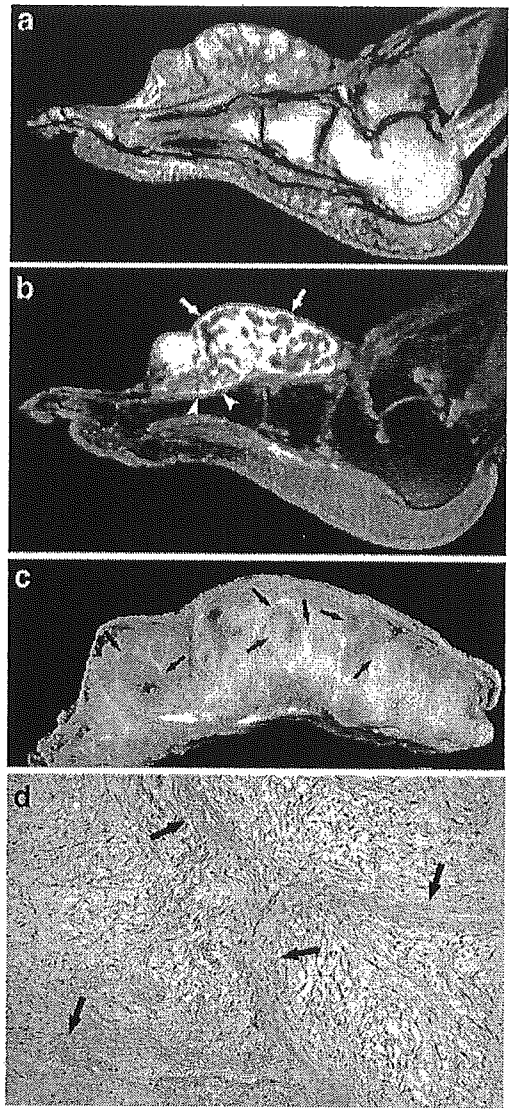


**Fig. 2** A 76-year-old woman with the EWS-CHN variant of EMC of the foot. **a** Sagittal, T2-weighted (3,000 ms/102 ms), MR image shows a well-defined mass, involving the foot, with high signal intensity greater than that of subcutaneous fat. **b** Sagittal, fat-saturated, T1-weighted (600 ms/15 ms), MR image after contrast administration shows peripheral enhancement (*arrows*). Also noted is extracompartmental growth beyond fascia (*arrowheads*). **c** Sagittally sectioned gross specimen shows myxoid and gelatinous nodules separated by fibrous septa (*arrows*). **d** Photomicrograph of the specimen demonstrates mature hyaline cartilage with fibrous tissue and myxoid stroma corresponding to the MRI appearance (H & E, original magnification ×100)

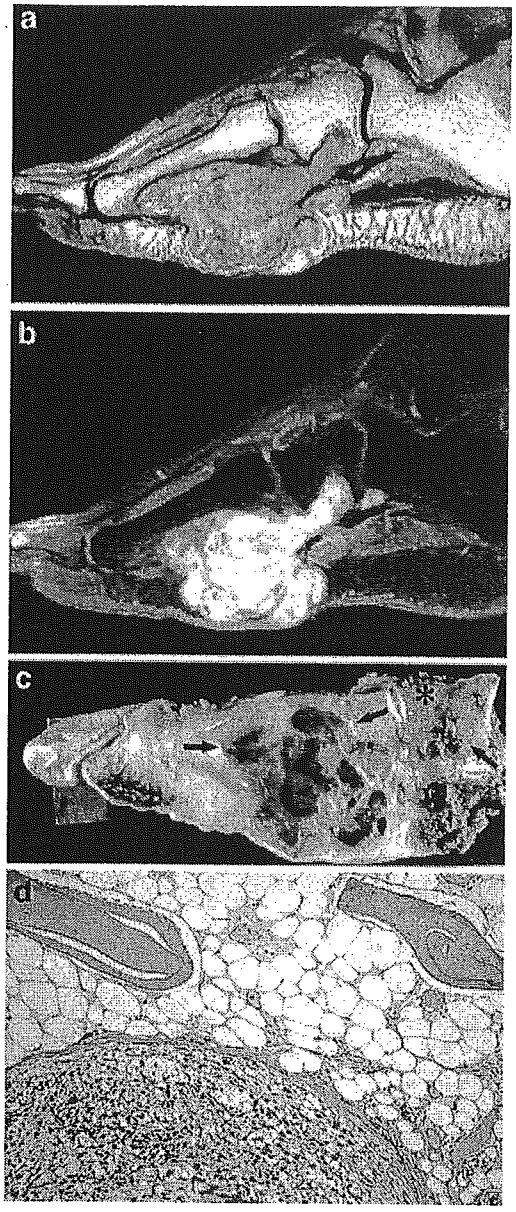


**Fig. 3** A 61-year-old woman with the TFG-TCH variant of EMC manifesting as extracompartmental extension. **a** Sagittal, T2-weighted (4,000 ms/89.9 ms), MR image shows a poorly defined mass involving the sole, with intermediate signal intensity less than that of subcutaneous fat. **b** Sagittal, fat-saturated, T1-weighted (600 ms/15 ms), MR image after administration of contrast material shows diffuse enhancement. **c** Sagittal plane of pathology specimen reveals extracompartmental growth (*arrows*) and destruction of calcaneous bone (*asterisk*). **d** Photomicrograph of the specimen shows nodular architecture of marrow invasion (H & E, original magnification ×100)

or TFG-TCH variants showed invasion of extracompartmental structure, bone, or vessels.

Gross characteristics of resected specimens featured multi-nodular architecture corresponding to the cross-sectional MRI features. In all cases the cut surface of specimens revealed myxoid and gelatinous nodules separated by fibrous septa, which corresponded to the appearance of various signal characteristics on T1-weighted and T2-weighted MR images. Fibrous septa also corresponded to areas of peripheral enhancement on contrast-enhanced MR images. Heterogeneous enhancement on contrast-enhanced MR images also correlated with the presence of intratumoral cysts ($n$=4) and hemorrhage ($n$=1). These areas corresponded to areas of high signal intensity on T2-weighted MR images. Geographic areas of necrosis were present in five patients (26%). Lobules often showed higher cellularity at the periphery, which corresponded to peripheral or diffuse enhancement on contrast-enhanced MR images. Hyaline cartilage had developed in one patient, although there were small islands of immature cartilage in several patients. All tumors were characterized microscopically by cords or clusters of neoplastic cells, which demonstrated a modest amount of eosinophilic, granular-to-vacuolated cytoplasm and uniform ovoid nuclei. Fourteen tumors were assigned grade 1 malignancy, and the remaining six tumors were grade 2.

All patients underwent surgical resection as a primary therapy. Surgical margins were adequate in 11 patients and inadequate in four. All patients with inadequate surgical margins had undergone subsequent wide resection. Chemotherapy (carboplatinum 1,000 mg, Adriamycin 60 mg) and radiotherapy (50 Gy) were included in the treatment regimen of one patient. The median follow-up period of all cases was 61 months. There were local recurrences in three patients (16%) at a median interval of 12 months. Metastases occurred in three cases (16%). The sites of metastases were lungs ($n$=3) followed by bone ($n$=1). Two patients that were being followed-up had died from the disease; 17 patients were alive with the disease or with no evidence of disease.

## Discussion

EMC has been described as a rare, adult, soft-tissue sarcoma. It commonly affects patients aged 50–60 years but is also known to occur in younger people [1, 2]. Patients usually present with non-specific symptoms, including tenderness and palpable mass [1–4]. Patient demographics and clinical symptoms in our series were similar to those in previous studies [1, 2].

Unlike in the previous reports [12–14], signal characteristics on T1-weighted MR images were varied. In our study, tumors showed predominantly low (5%), intermediate (80%), or high (15%) signal intensity relative to muscle on T1-weighted MR images. These features on T1-

weighted MR images might be due to underlying pathologic changes. In all our cases, myxoid and gelatinous nodules, separated by fibrous septa, were frequently apparent on pathologic observation. Pathologically, EMC often consists of hemorrhagic changes [2]. MRI evidence of hemorrhagic foci of high signal intensity on T1-weighted image was seen in one of our patients. Although this was in accordance with pathologic findings, the occurrence of hemorrhage was not a common finding on MR images.

A few case series have demonstrated homogeneous or heterogeneous enhancement on contrast-enhanced MR images [12–14]. In fact, all our cases showed heterogeneous enhancement. Peripheral enhancement was also found in 32% of our cases after administration of contrast material at MRI. These results suggest that the enhancement pattern on MR images may depend on tumor heterogeneity in EMC. The high frequency of peripheral enhancement that was demonstrated on contrast-enhanced T1-weighted MR images was in good accordance with the gross pathologic features.

High signal intensity on T1- weighted images corresponded to areas of hemorrhage identified pathologically, as described in our study. Although intratumoral hemorrhage was found in only one case, hemorrhagic soft-tissue sarcoma could be considered in the differential diagnosis. Synovial sarcoma is often associated with hemorrhagic change, representing various MR signal patterns. Triple-signal pattern, one of the heterogeneous patterns on T2-weighted MR images, is considered to be not specific but suggestive of the diagnosis, given the most prevalent age [15]. Fluid–fluid levels may occur whenever substances of differing densities are contained within a cystic or compartmentalized structure. The levels are depicted when imaging is performed in a gravity-dependent plane. The presence of fluid–fluid levels in soft-tissue tumors cannot be considered diagnostic of any particular tumor, including synovial sarcoma and malignant fibrous histiocytoma [16]. A sign of fluid–fluid level was seen in none of our cases on T2-weighted MR images, which would suggest that this finding might be less frequent in patients with EMC.

The identification of the highly specific balanced chromosomal rearrangement in EMC provides a valuable tool for diagnosis at the molecular level. In our series, 68% of tumors consisted of three variant fusions. The relationship between cytogenetic variants and imaging findings were not fully understood. Although signal characteristics on T1-weighted and T2-weighted MR images were non-specific, peripheral enhancement on contrast-enhanced MR images was seen more frequently in tumors with the EWS-CHN variant than in those with other cytogenetic variants, according to our results. Peripheral enhancement on contrast-enhanced MR images may be characteristic for this entity, because most patients with EMC have chromosomal aberration of EWS-CHN [6–11].

The imaging features of EMC reflect the underlying pathologic findings [12–14]. Extracompartmental extension and cortical destruction, with soft-tissue mass, were found in 26% of cases, according to our results. In addition, all tumors with TAF2N-CHN or TFG-TCH variants showed invasion of extracompartmental structure, bone, or vessels. Although the association between imaging findings and cytogenetic variants is obscure, the invasive nature of MRI findings may be characteristic in these variants.

As with other soft -tissue sarcomas in adults, surgical resection is recommended in EMC. EMC typically has a prolonged clinical course with complete resection [4]. However, the behavior of EMC has been reported to be poor, with frequent local recurrences and distant metastases [1, 3]. Sixteen percent of our patients developed local recurrences, and metastases occurred in 16% of our cases. EMC seems to have frequent recurrences and metastases, and long-term follow-up is needed.

We recognize certain limitations of our study. Because of the referral basis of our cases, we were unable to control the MRI parameters. However, our retrospective review includes a greater number of cross-sectional imaging studies than does any previous study [5–8]. Despite these limitations, our study may add substantial understanding of imaging features of EMC.

## Conclusion

Characteristic imaging features of EMC are multi-nodular soft-tissue masses, presenting predominantly hyper-signal intensity on T2-weighted MR images and heterogeneous enhancement after administration of contrast material. Peripheral enhancement was seen more frequently in tumors with the EWS-CHN variant than in those with other cytogenetic variants. Tumors with TAF2N-CHN or TFG-TCH variants showed invasion of extracompartmental structure, bone, or vessels. These features clearly reflect the underlying histopathologic characteristics of EMC.

## References


1. Saleh G, Evans HL, Ro JY, Ayala AG. Extraskeletal myxoid chondrosarcoma. A clinicopathologic study of ten patients with long-term follow-up. Cancer 1992;15 70:2827–30
2. Meis-Kindblom JM, Bergh P, Gunterberg B, Kindblom LG. Extraskeletal myxoid chondrosarcoma: a reappraisal of its morphologic spectrum and prognostic factors based on 117 cases. Am J Surg Pathol 1999;23:636–50
3. Lucas DR, Fletcher CD, Adsay NV, Zalupski MM. High-grade extraskeletal myxoid chondrosarcoma: a high-grade epithelioid malignancy. Histopathology 1999;35:201–8

*Jpn J Clin Oncol 2005;35(8)444–452*
*doi:10.1093/jjco/hyi128*

# Incidence of Multiple Primary Malignancies in a Cohort of Adult Patients with Soft Tissue Sarcoma

**Ukihide Tateishi[1], Tadashi Hasegawa[2], Seiichiro Yamamoto[3], Umio Yamaguchi[4], Ryohei Yokoyama[5], Hiroshi Kawamoto[3], Mitsuo Satake[1] and Yasuaki Arai[1]**

[1]Diagnostic Radiology Division, [2]Pathology Division and [4]Orthopedic Surgery Division, National Cancer Center Hospital and Institute, [3]Statistics and Cancer Control Division, Research Center for Cancer Prevention and Screening, National Cancer Center, Tokyo and [5]Department of Orthopedic Surgery, Kyushu Cancer Center, Fukuoka, Japan

Received March 6, 2005; accepted June 1, 2005; published online July 15, 2005

**Objective:** Some studies to date have suggested the development of multiple primary malignancies in patients with soft tissue sarcoma. The current study was performed to quantify the risk of development of multiple primary malignancies in adult patients with soft tissue sarcoma.
**Methods:** A total of 406 consecutive patients who were diagnosed with soft tissue sarcoma were identified in the study analysis. The cumulative incidence of multiple malignancies was calculated by comparing Kaplan–Meier curves and log-rank tests from each histological type. A Cox proportional hazards model was used to estimate the influence on the hazard ratio (HR) of each variable.
**Results:** A total of 35 patients with soft tissue sarcoma (9%), having preceding ($n = 15$) and subsequent ($n = 20$) malignancies other than soft tissue sarcoma were documented. The 5- and 10-year estimated cumulative incidence of multiple primary malignancies were 7.6 and 12.3%, respectively. The hazard risk of multiple primary malignancies adjusted for potential confounding variables was significantly associated with age at diagnosis (HR = 1.51, $P = 0.0019$). The risk of multiple primary malignancies was also increased in patients with myxofibrosarcoma adjusted by the potential confounding variables (HR = 2.34, $P = 0.048$). The 5- and 10-year estimated cumulative incidence of multiple primary malignancies in patients with myxofibrosarcoma were both 16.9%.
**Conclusion:** The results of our study confirm that the risk of multiple malignancies appears to be impacted by age at the time of diagnosis of the first tumor and by the histological type of myxofibrosarcoma.

*Key words: soft tissue sarcoma – myxofibrosarcoma – multiple malignancies – second primary tumor*

## INTRODUCTION

The development of multiple malignancies in a single individual has been reported after successful treatment of primary tumors (1,2). The greatest attention has been focused on second primary tumors (SPTs) after treatment of malignant lymphoma (3), retinoblastoma (4) and malignant germ cell tumor (5,6) because good cure rates have been achieved for many years, resulting in many long-term survivors.

The occurrence of multiple malignancies in patients with soft tissue sarcoma (STS) has also been reported (7,8). Studies focused on patients with osteosarcoma have revealed an overall 10-year cumulative incidence of SPT of 2.0–3.1% (9,10). Adult patients with STS have been found to develop other malignant neoplasms either before or after the diagnosis of STS, and this phenomenon occurred at a significantly higher rate than reported for the occurrence of STS in the general cancer population (11).

However, the risk of SPT after treatment of the first tumor has been mainly described in children with STS. Although we have observed the occurrence of multiple primary malignancies that occurred in adult patients with various histological types of STS, especially pleomorphic malignant fibrous histiocytoma (MFH) and myxofibrosarcoma, in daily clinical practice there has been little information on the management of these patients. The current study was therefore undertaken to assess the risk of development of another primary malignant tumor in adult patients with STS.

## MATERIALS AND METHODS

### PATIENTS

The records of 500 consecutive adult STS patients diagnosed and treated between February 1962 and August 2003 were

For reprints and all correspondence: Ukihide Tateishi, Division of Diagnostic Radiology, National Cancer Center Hospital, 5-1-1, Tsukiji, Chuo-ku, 104-0045 Tokyo, Japan. E-mail: utateish@ncc.go.jp

retrieved from the pathology files of our institution. This study was approved by the local Ethics Committees after confirmation of informed consent by the patients to a review of their records and images. The enrollment criteria consisted of (i) adult STS patients whose pathological specimens and medical charts were available for review; and (ii) patients who were not lost to follow-up. The exclusion criteria consisted of (i) subjects whose pathological specimens and medical charts were insufficient for review; and (ii) subjects whose pathological subtypes were considered to be rare in the clinical setting. Thus, 94 patients (19%) whose tumors comprised epithelioid sarcoma ($n$ = 25), alveolar soft part sarcoma ($n$ = 20), clear cell sarcoma ($n$ = 16), extraskeletal myxoid chondrosarcoma ($n$ = 20) or extraskeletal osteosarcoma ($n$ = 13) were excluded from the analysis, and the 406 patients with common STSs were included in the analysis. The patients consisted of 223 men and 183 women, and they ranged in age from 16 to 87 years (median age: 53 years). During the period 1962–2003, the concept of MFH or myxofibrosarcoma changed. Twenty-three myxofibrosarcomas (34%) which were previously diagnosed as myxoid variant of MFH or solely fibrosarcoma were reclassified by the review of pathological examinations. Autopsy was performed in 16 cases (4%) and their pathological specimens were also available for review.

In the patients who developed multiple primary malignancies, we investigated: age at diagnosis, gender, family history, anatomic site, tumor size, depth, surgical margin, histological type, MIB-1 score, grade, whether chemotherapy has been performed, whether radiation therapy has been performed and the outcome. If the patient had died, the date and the cause of death were also noted.

Patients were followed-up with regard to survival until August 31, 2004, at which time 250 patients were alive with no evidence of disease, 26 patients were alive with disease and 130 patients had died of their disease. The malignancy-free survival period (MFSP) was measured from the date of diagnosis of STS to the date of the first observations of multiple malignancies. If the detection of malignancy other than STS preceded the date of diagnosis of the STS, the MFSP was recorded as 0. If a patient was alive without developing any multiple malignancies at the last visit, the data on MFSP were censored as of the date when the survival was confirmed. If a patient died without detection of other primary malignancies, the MFSP was censored at the date of death. If other primary malignancy was found at autopsy, the date of death was treated as an event.

Histological slides of the primary tumors of all patients were reviewed for diagnosis by two experts. Whenever necessary, immunohistochemistry was used to confirm the diagnosis or tumor type according to the WHO classification (12). MIB-1 immunostaining was performed to grade all tumors. An MIB-1 score of 1 was assigned to lesions with an MIB-1 labeling index (LI) of 0–9%, an MIB-1 score of 2 was given to lesions with an MIB-1 LI of 10–29%, and an MIB-1 score of 3 was given to lesions with an MIB-1 LI $\geqslant$ 30%. There were tumors with an MIB-1 score of 1 ($n$ = 140; 35%), 2 ($n$ = 62; 15%) and 3 ($n$ = 204; 50%). The histological grade is a three-grade system obtained by adding the scores for tumor differentiation, tumor necrosis and MIB-1 score, each of which was given a score of 0–3 (13). By using the grading system, tumors corresponded to grade 1 ($n$ = 128; 32%), grade 2 ($n$ = 107; 26%) and grade 3 ($n$ = 171; 42%), respectively. Tumor depth was measured relative to muscular fascia that had been invaded and was characterized as superficial or deep. The vast majority of lesions ($n$ = 322; 79%) were deep seated, and 94 tumors were superficial.

### Statistical Analysis

Univariate analysis of the cumulative incidence of multiple malignancies was performed by comparing Kaplan–Meier curves and log-rank tests from each histological type. The hazard ratio (HR) of each variable was estimated by using a Cox proportional hazards model in the univariate and multivariate analyses. The following factors are considered as potential confounding factors for the incidence of multiple malignancies: age at presentation, gender, family history of malignant neoplasm, anatomic site, tumor size, depth, surgical margin, histological type, MIB-1 score (1, 2 or 3) and grade (1, 2 or 3). Variable selection by the backward elimination ($\alpha$ = 0.2) procedure was performed in the multivariate analyses. All analyses were performed with SAS Software (version 6.12; SAS Institute, Cary, NC).

## RESULTS

Tumors had a diameter >5 cm in 302 patients (74%). Most tumors were located in the extremities ($n$ = 244; 60%) compared with the trunk ($n$ = 96; 24%) and other sites ($n$ = 66; 16%). The histological types consisted of liposarcoma ($n$ = 159; 39%), myxofibrosarcoma ($n$ = 67; 17%), pleomorphic MFH ($n$ = 53; 13%), synovial sarcoma ($n$ = 50; 12%), leiomyosarcoma ($n$ = 32; 8%), malignant peripheral nerve sheath tumor (MPNST; $n$ = 25; 6%) and fibrosarcoma ($n$ = 20; 4%). Of these 406 tumors, 371 tumors (91%) did not develop multiple malignancies (Table 1).

A total of 35 patients (9%) with STS were documented in the study population, among whom the STS was preceded by ($n$ = 15) and followed by ($n$ = 20) malignancies other than STS. The median age at the time of diagnosis of the first tumors was 63 years (range 39–79 years). The SPTs were diagnosed a median of 64 months after the diagnosis of the first tumor. A third primary tumor (TPT) was found in eight patients, a median of 127 months after the first tumor. One patient was found to have a fourth primary tumor 331 months after the first tumor. The overall 5- and 10-year estimated cumulative incidence of multiple primary malignancy was 7.6% [95% confidence interval (CI) 4.7–10.4] and 12.3% (95% CI 7.4–18.0), respectively.

Information related to the patients is listed in Table 2. The most frequent histological types of STS were myxofibrosarcoma ($n$ = 13; 19.4%) and pleomorphic MFH ($n$ = 6; 11.3%).